

Membrane-activated microfluidic rotary devices for pumping and mixing

Hao-Yu Tseng · Chih-Hao Wang ·
Wang-Ying Lin · Gwo-Bin Lee

Published online: 16 May 2007
© Springer Science + Business Media, LLC 2007

Abstract Microfluidic devices are operated at a low-Reynolds-number flow regime such that the transportation and mixing of fluids are naturally challenging. There is still a great need to integrate fluid control systems such as pumps, valves and mixers with other functional microfluidic devices to form a micro-total-analysis-system. This study presents a new pneumatic microfluidic rotary device capable of transporting and mixing two different kinds of samples in an annular microchannel by using MEMS (Micro-electro-mechanical-systems) technology. Pumping and mixing can be achieved using a single device with different operation modes. The micropump has four membranes with an annular layout and is compact in size. The new device has a maximum pumping rate of 165.7 $\mu\text{L}/\text{min}$ at a driving frequency of 17 Hz and an air pressure of 30 psi. Experimental data show that the pumping rate increases as higher air pressure and driving frequency are applied. In addition, not only can the microfluidic rotary device work as a peristaltic pumping device, but it also is an effective mixing device. The performance of the micromixer is extensively characterized. Experimental data indicate that a mixing index as high as 96.3% can be achieved. The developed microfluidic rotary device can be easily integrated with other microfluidic devices due to its simple and reliable PDMS fabrication process. The development of the microfluidic rotary device can be promising for micro-total-analysis-systems.

Keywords Microfluidics · Micropump ·
Micromixer · MEMS

H.-Y. Tseng · C.-H. Wang · W.-Y. Lin · G.-B. Lee (✉)
Department of Engineering Science,
National Cheng Kung University, Tainan, Taiwan 701
e-mail: gwobin@mail.ncku.edu.tw

Nomenclature

C	Concentration
CCD	Charge coupled device
C_o	Initial fluorescent concentration
C^+	Normalized concentration ($=C/C_o$)
C_∞	Normalized complete mixed concentration ($=0.5$)
DI	Deionized
ELISA	Enzyme-linked immunosorbent assay
EMV	Electromagnetic valve
f_{EMV}	Driving frequency of the electromagnetic valve (Hz)
f_{mixing}	Driving frequency of the rotary micromixer (Hz)
FITC	Fluorescein isothiocyanate
H	Channel width
LCD	Liquid crystal display
MEMS	Micro-electro-mechanical-systems
PDMS	Polydimethylsiloxane
PR	Photoresist
X	Longitudinal coordinate
Y^+	Normalized transversal coordinate ($=y/h$)
Y	Transversal coordinate
σ	Mixing index

1 Introduction

In the past decade, micromachining technology has provided a promising means to miniaturize instrumentation for chemical analysis and biomedical applications. Transportation and mixing of fluids in the microchannels has been critical for miniaturized biomedical systems. Many micro-pumping devices have been extensively explored recently (Gravesen et al. 1993). For example, electroosmotic micro-pumps using electrokinetic forces to transport samples were

reported (Zeng et al. 2001). A flow rate of $3.6 \mu\text{L}/\text{min}$ can be achieved at a voltage of 2,000 V. Pneumatic micropumps fabricated by multilayer soft lithography techniques were also employed to drive microfluids (Unger et al. 2000). The pneumatic membrane-type micropump can provide reasonable pumping rates and back pressures. Alternatively, piezoelectric micropumps were reported to be a promising candidate to drive fluid in the microchannel (Husband et al. 2004). However, it can be challenging to deposit thin-film piezoelectric materials integrated with micromachined structures. Even though the piezoelectric micropump has a high pumping rate, a relatively complex control circuit, a high driving voltage, and high temperatures during operation may pose a challenge for its use in biomedical applications. Magnetic micropumps driven by external magnetic forces were also reported (Yamazaki et al. 2003a,b). Typically, a spiral-type magnetic mechanical structure was designed into the microchannel and rotated by the external magnetic gradient to transport the fluids (Yamazaki et al. 2003a,b). The maximum pressure produced by the spiral-type microstructure is 70 Pa. Therefore, the magnetic micropump can be used in the low-Reynolds-number microdevice (Yamazaki et al. 2003a,b). Among these micropumps, the pneumatic membrane-type micropump is one of the most commonly used and reliable devices. Typically, deformation of membranes induces the change of the chamber volume, thus driving the fluid to move in the microchannel. Normally, three membranes driven peristaltically were used for pneumatic micropumps (Fu et al. 2002). Rotary pneumatic micropumps have also been demonstrated (as shown in Fig. 1(a); Chou et al. 2000, 2001). The rotary micropumping device could drive the fluid clockwise or counterclockwise inside the annular channel. In their work, the annular channel can be also used as a mixing device while incorporated with two additional pneumatic micropumps (pumps #3 and #4 in Fig. 1(a)). Two mixing mechanisms, including a fixed-volume and a continuous-flow mixing, were successfully demonstrated. For the fixed-volume mixing, samples first fill the annular channel and then the rotary pump moves the samples along the annular channel for 30 s such that the samples could be well mixed. During the mixing process, two additional microvalves are shut off to isolate the rotary mixing. Continuous-flow mixing is almost the same as the fixed-volume mixing. The only difference is that samples are drawn into the rotary section by another two pneumatic micropumps (pumps #1 and #2 in Fig. 1(a)), and then mixed by the rotary pump. Apparently, relatively complicated microstructures are required to achieve pumping and mixing. Moreover, each pneumatic pump is operated by using peristaltic motion of three PDMS membranes. Four-pump layout requires at least twelve electromagnetic valve (EMV) switches.

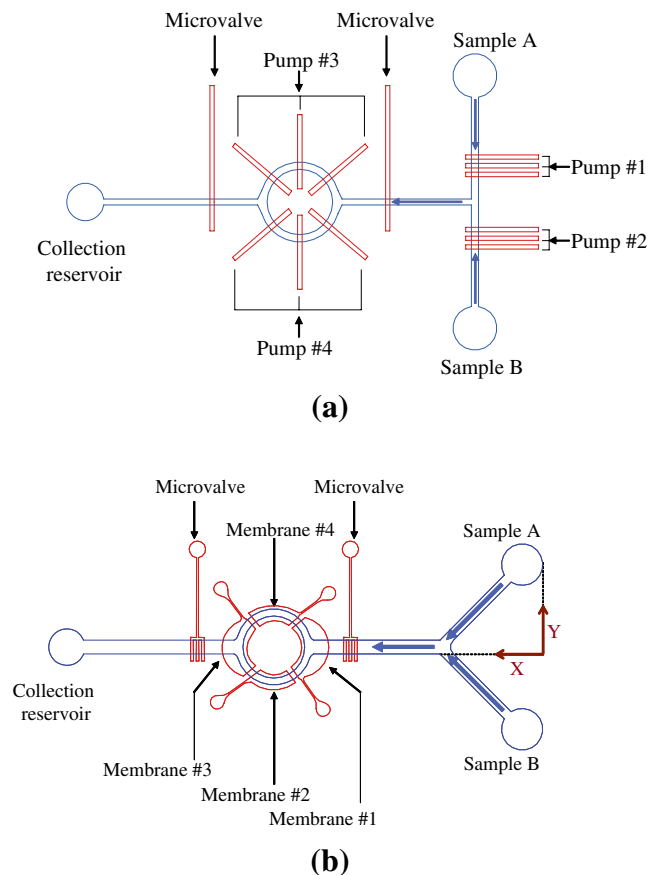


Fig. 1 (a) Schematic illustration of a rotary pumping device comprising four pneumatic micropumps and two microvalves (Chou et al. 2000, 2001). Pumps #1 and #2 are used to control the transportation of fluids. Alternatively, pumps #3 and #4 drive the fluid clockwise or counterclockwise in the annular channel. Two valves are used during the mixing process. (b) Schematic illustration of the proposed microfluidic rotary device composed of a Y-shaped microchannel, four PDMS membranes and two pneumatic microvalves

Similarly, a rotary microfluidic device for polymerase chain reaction was reported (Liu et al. 2002). There were four pneumatic micropumps used to transport the samples in this developed chip. Two of the pumps could rotate the samples at a rate of two to three revolutions per minute. However, controlling the flow in the peristaltic pneumatic micropumps usually requires the use of three EMV switches. Recently, this research group reported a serpentine-shape pneumatic micropump. With a proper design, fluids can be driven by the peristaltic action of membranes located at the intersections of the fluidic microchannel and the serpentine-shape microchannel (Wang et al. 2005). The micropump provides an improved pumping rate and is controlled by using a single EMV switch. ELISA (Enzyme-linked immunosorbent assay)-based diagnosis was also successfully performed by using this pneumatic micropump.

Meanwhile, microfluidic devices are usually used in chemical reaction systems or bio-detection systems. Therefore a rapid and efficient mixing device is also in great need. However, due to the low-Reynolds-number nature of the fluid flow, it is challenging to enhance the mixing in the micro-scale system. For mixing two confluent samples in a micro-channel, many methods have been reported by using MEMS technology in the literature (Nguyen and Wu 2005). In general, micro-scale mixing can be divided into two main categories to generate transverse flows for the enhancement of the mixing efficiency, namely active and passive mixers. Typically, passive mixers use the channel geometry either to laminate the flowing fluids or to generate chaotic advection in these fluids. Both approaches lead to an increase in the interface between two fluids and consequently to achieve a better mixing. Their advantage is that they do not need external energy. Deformation of microchannels and specially designed obstacles are usually used in the passive micromixers. For example, laminate mixers which split the inlet streams into several laminated streams were reported (Miyake et al. 1997). Microchannels with twisted and sandwiched structures were demonstrated as mixers (Hinsmann et al. 2001). Serial laminated mixers which joined laminated streams vertically could also successfully mix the fluids (Kochy et al. 1998; Munson and Yager 2004; Gray et al. 1998). Generally speaking, laminate micromixers increase the mixing interface surface to enhance the mixing efficiency. In contrast, another type of passive micromixers can generate chaotic advection in the microchannel. By splitting or breaking the microfluids, transversal mixing inside the channel can be achieved (Hessel et al. 2003; Hardt et al. 2003). Usually, arranging obstacles in the microchannel is the most common way to induce chaotic advection (Wang et al. 2002). For example, a microfabricated silicon-based micromixer with pillars inside the microchannel was reported (Lin et al. 2003). Other approaches using different patterns on the floor of the microchannel were utilized to improve mixing efficiency (Li and Chen 2005; Park et al. 2004; Song et al. 2003; Stroock et al. 2002).

Alternatively, active micromixers require external power supplies to enhance mixing (Nguyen and Wu 2005). For example, pressure disturbances caused by an external force to induce an irregular distribution of hydraulic pressure in the microchannel were demonstrated as a micromixer (Glasgow and Aubry 2003). A silicon-based magnetic micromixer with embedded electrodes was successfully formed to increase the mixing performance (Suzuki and Ho 2004). Buried electrodes were also used by the current research group to generate the capacitance effect and to change the surface zeta potential inside the microchannel. Then the alternating electric field in the microchannel could result in the chaotic advection of the fluids (Lee et al. 2004). Similarly, acoustic activation and

thermal forces were also used for enhancing the mixing (Katoua et al. 2005; Yang et al. 2000; Tsai and Lin 2002).

In this study, we present a new micro rotary device, which could transport and mix the samples by using the same microstructure. Using only four membranes (Fig. 1(b)), the device could control pumping and mixing. In other words, two devices, a pump and a mixer, were combined together. We report an active device comprising of PDMS (polydimethylsiloxane) membranes with an annular layout to perform pumping and mixing. The PDMS was chosen because of its resilient properties allowing for precise membrane deflection even after many deformation cycles (Duffy et al. 1999). Four PDMS membranes with an annular layout were used to produce the pumping effect by activating them in a specific sequence. In addition to the micropump, the same device can be also used as a micromixer by using a different operation sequence. The new microfluidic rotary device can transport and mix samples by using four controllable membranes and two special control sequences. The pumping rate and the mixing efficiency of the rotary device have been experimentally explored. Experimental data show that the developed device can successfully transport and mix the samples.

2 Experimental

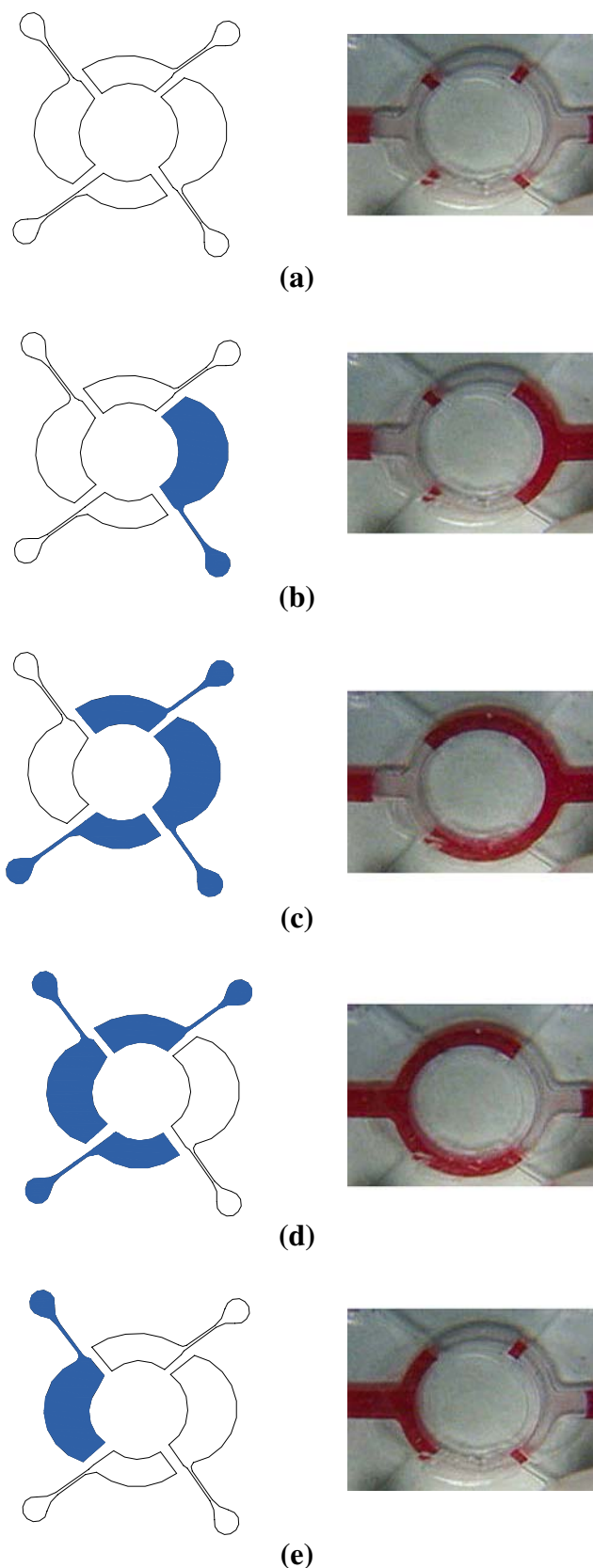
2.1 Design

The major contribution of the current study is the design and fabrication of a new pneumatic peristaltic rotary device capable of pumping and mixing. Previous study used a complicated microstructure to achieve pumping and mixing (Fig. 1(a)). In this study, we adopted a simpler design such that the developed device is compact in size. Figure 1(b) shows a schematic illustration of the microfluidic rotary device composed of a Y-shaped microchannel, four PDMS membranes and two pneumatic microvalves. The dimensions of the chip are measured to be 4.5 cm in length and 1.3 cm in width. Several dimensions of the devices have been designed and fabricated to test which dimension can provide satisfactory performance for pumping and mixing. Finally, the width and depth of the Y-shaped channel and the annular channel were determined to be 500 and 100 μm , respectively. The dimensions of the connected channel were 1,000 μm in width and 100 μm in depth. The depth of the microvalve was 100 μm . Each microvalve was composed of three finger-shaped membranes with a width of 200 μm such that it could stop the movement of fluids in the liquid microchannel. The inner and the outer radius of the annular channel underneath the PDMS membranes are 2,250 and 2,750 μm , respectively. In this study, the

Fig. 2 A series of pictures showing the pumping process. The left-hand side of each picture shows an illustration of the four membranes and the right-hand side shows the fluid motion observed under a microscope. The pump operation sequence in (a), (b), (c), (d), and (e) are 1111, 0111, 0010, 1000 and 1101, respectively

microfluidic rotary device is designed with two functions, pumping and mixing. Samples can be injected from reservoirs A and B and then pumped to the annular channels. Then, samples can be mixed in a rotary fashion; driven by the deformation of each membrane. Two pneumatic microvalves are used to control the fluids, if necessary. Four PDMS membranes are driven by four EMVs (model SD70M-6BG-32, SMC, Japan) which can be programmed in a variety of sequences by using a microcontroller (8051 microcontroller, model AT89C51 24PC, ATMEL, USA). Peristaltic pumping is achieved by the time delay activation of the series of membranes. For example, the membranes shown in Fig. 2 can be driven peristaltically using five different operating sequences (1111, 0111, 0010, 1000, and 1101) to generate the pumping effect. Note that “1” represents that external compressed air is applied and the PDMS membrane is deformed. Conversely, “0” corresponds to a null condition. The position of the four digits represent membranes 1, 2, 3, and 4, respectively. For example, 1101 indicates that membranes 1, 2, and 4 are deformed by external compressed air and membrane 3 is not activated. With this approach, fluids can be pumped from the right to left as shown in Fig. 1(b). Figure 2 illustrates a full cycle of the pumping process and shows a series of images taken under a microscope. At first, all membranes are deformed (1111). Then the first membrane is released and the sample (red ink) is extracted to fill in the first chamber (0111). By using an appropriate operation sequence on the four membranes (1111, 0111, 0010, 1000, and 1101 as shown in Fig. 2), samples can be pumped from the left to the right. The pumping rate can be controlled by changing the applied pressure of the compressed air and the driving frequency of the membranes.

Alternatively, another operation sequence (0011, 1001, 1100 and 0110) can be used to mix confluent samples in a clockwise fashion as shown in Fig. 3. This sequence can drive confluent flows along the annular microchannel such that centrifugal forces can be used for mixing. The moving speed of the confluent flows and the deformation of the membranes can affect the mixing efficiency. More importantly, these two functions of pumping and mixing can be achieved simultaneously by using an appropriate sequential control of the membranes. For example, a sequence of 1111, 0111, 0010, 0011, 1001, 1100, 0110, 1000, and 1101 can be used to transport and mix the sample at the same time.



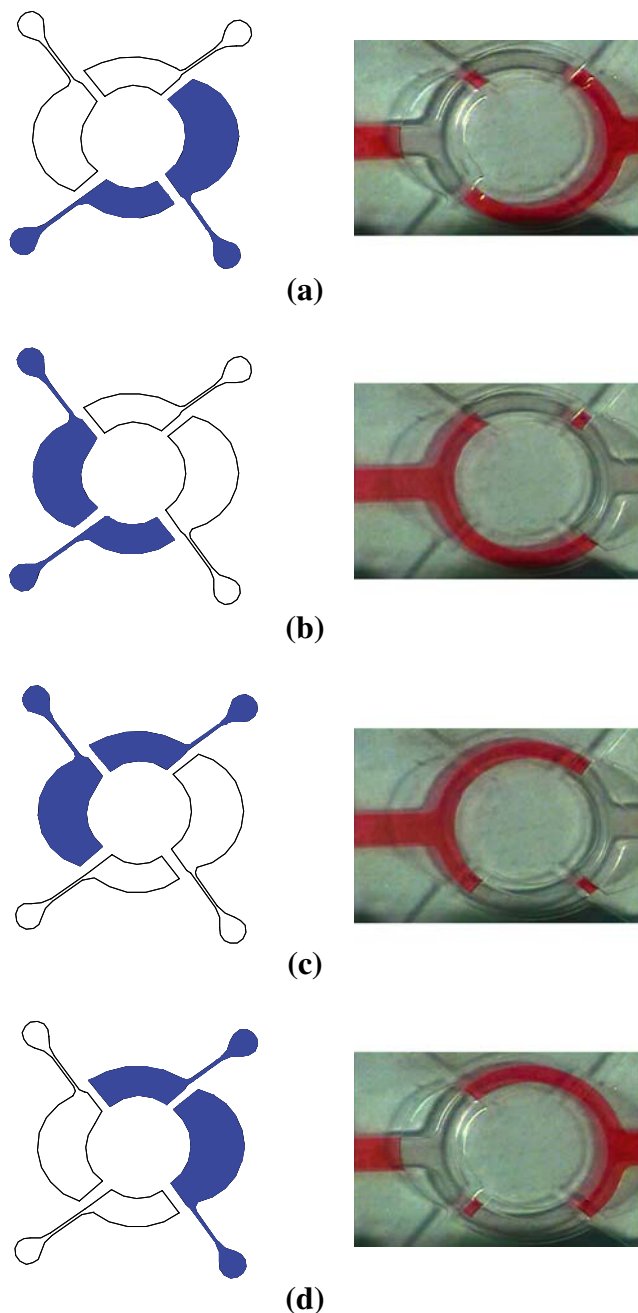


Fig. 3 A series of pictures showing the process of mixing. The pump operation sequence in (a), (b), (c) and (d) are 0011, 1001, 1100 and 0110, respectively

2.2 Fabrication

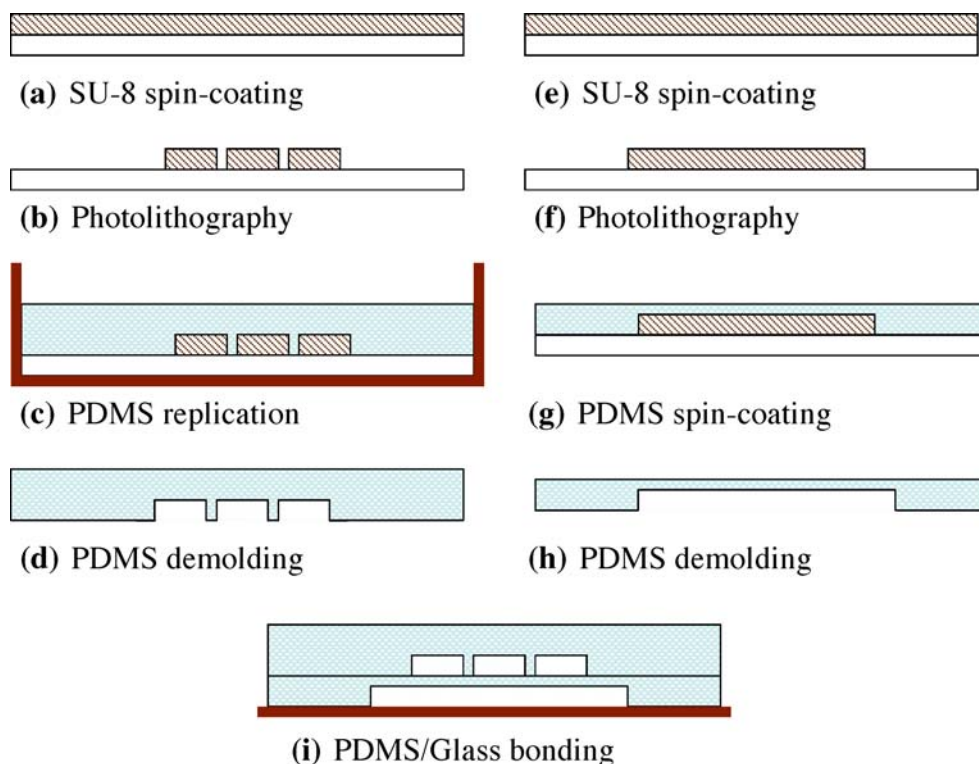
The rotary micropump and micromixer are made of three layers comprising of a glass substrate and a double-layer PDMS structure. The double-layer PDMS structure consists of a thick layer and a thin layer. The thick layer (500 μm) is designed to have an air chamber for connection to an external air pressure source and the thin layer (100 μm) is for easy deformation. The double layers of PDMS are

fabricated to form the microchannel, microvalves and membranes (as shown in Fig. 1(b)). Figure 4 shows a schematic representation of the microstructure fabrication process by using soft lithography processing (Sia et al. 2003). There are five major steps involved, namely SU-8 spin-coating, photolithography, PDMS replication, PDMS demolding from the template and PDMS/glass bonding processes (Ziaie et al. 2004). Briefly, the template was formed on a silicon substrate by using a standard lithography process. At first, SU-8 (50) (NANO[®], MicroChem, USA) negative thick PR (photoresist) was spin-coated on a silicon wafer at 1,000 rpm before a soft bake process. Note that the uniformity of the SU-8 coated surface is crucial for the subsequent bonding process. Then, two steps of the soft baking process, 65°C for 30 min and 95°C for 10 min, were performed. After soft baking, a standard lithography was executed with an exposure dose of 600 mJ cm^{-2} for 45 s to define the microstructure. SU-8 was then developed to obtain a SU-8 template. Post exposure baking at 95°C for 10 min and flood exposure after development was performed to assure a well-defined microstructure. Then, a double-layer microfluidic structure was formed by using a PDMS casting fabrication process. Elastomer and curing agent (Sylgard 184A and 184 B, Sil-More Industrial Ltd., USA) were mixed thoroughly in the ratio of 10:1 and poured onto the SU-8 mold (as shown in Fig. 4(c)). A vacuum pump was used to eliminate air bubbles generated from the mixing of the elastomer and the curing agent. Likewise, a PDMS thin film template was formed by using a similar fabrication process (Fig. 4(g)). A thin PDMS layer was formed by spinning at 800 rpm. PDMS was then placed in a 75°C oven for 120 min for curing. Then a PDMS inverse microstructure was formed. After the casting process, the PDMS structure was peeled off the template mechanically (Fig. 4(d) and (h)). The thick and thin PDMS layers were treated with oxygen plasma. At last, the double-layer PDMS structure was aligned under a microscope and bonded with the glass substrate. Figure 5 shows a photograph of the microfluidic rotary device. The dimensions of the chip were measured to be 4.5 \times 1.3 cm.

2.3 Experimental setup

The motion of membranes was controlled by EMVs utilizing an 8051 microcontroller. Two different operation sequences, for pumping and mixing, respectively, were programmed. The driving frequency of the EMVs can be controlled by using the microcontroller. The PDMS membranes intersecting the fluid microchannel underneath can be deformed by the external air compressor (model DP0105-Y1-0001, NITTO KOHKI, USA), thus generating the pumping and valving effects. A hand-held system for integrating the controller, EMVs, an air

Fig. 4 A simplified fabrication process for the microfluidic rotary device



compressor, a LCD (liquid crystal display, model PVC160202BTL, PICVUE Electronics, Taiwan) panel and a keyboard has been developed. The images of the pumping and mixing can be acquired by using a CCD (charge coupled device, model TE/CCD512TKM, Roper Scientific Inc., USA) for the capturing of the pictures. The sample fluid used to test the micropump was red ink. For the characterization of the micromixer, 10^{-5} M FITC (fluorescein isothiocyanate) fluorescence dye (ANZ0109, Invitrogen, USA) and a 10^{-3} M CE buffer solution ($\text{Na}_2\text{B}_4\text{O}_7 \times 10\text{H}_2\text{O}$, sodium bicarbonate, Showa Chemical, Japan) were used to measure the mixing efficiency generated by the rotary micropump. While analyzing the experimental data, gray-scale pictures were used to characterize the performance of the mixer.

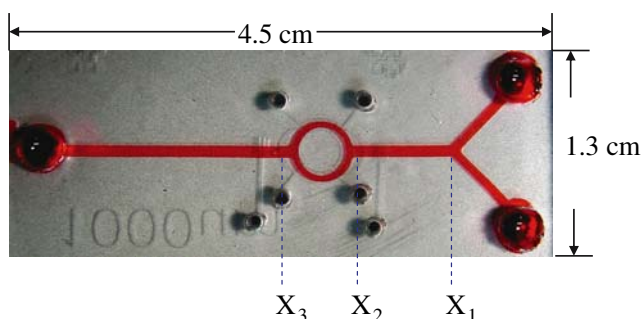


Fig. 5 Photograph of the microfluidic rotary device. The dimensions of the chip are 4.5 cm in length and 1.3 cm in width. The width of the channel is 1,000 μm . X_1 , X_2 and X_3 are 0.8, 1.7, and 2.3 cm, respectively

3 Results and discussion

3.1 Characterization of micropumps

Figure 2 illustrates the operation process of the rotary pumping device while the fluid is moved from the right to the left. The schematic illustration on the left-side side of Fig. 2 shows in details which membranes are activated by external air pressure. The photographs on the right-hand side show the corresponding images observed under a microscope. When the membranes were driven peristaltically using five different operating sequences (1111, 0111, 0010, 1000, and 1101) as described in Section 2.1, fluids can be successfully driven from the right to the left.

The pumping rate of the micropump was extensively investigated. Figure 6 shows the relationship between the pumping rate and the driving frequency at three different applied air pressure, 10, 20, and 30 psi, respectively. The pumping rate of the rotary pump increases with the increment of the driving frequency until it reaches a value of 17 Hz. The pumping rate starts to fall afterwards since the time required to activate the membranes is longer than the switching time of EMVs. In this case, the membranes cannot be activated completely to draw enough fluids and thus the pumping rate decreases accordingly. Figure 6 also reveals that the increase of air pressure also improves the pumping rate. Since the higher air pressure applied to the membranes could generate a bigger deformation of the membranes, the pumping rate is therefore enhanced.

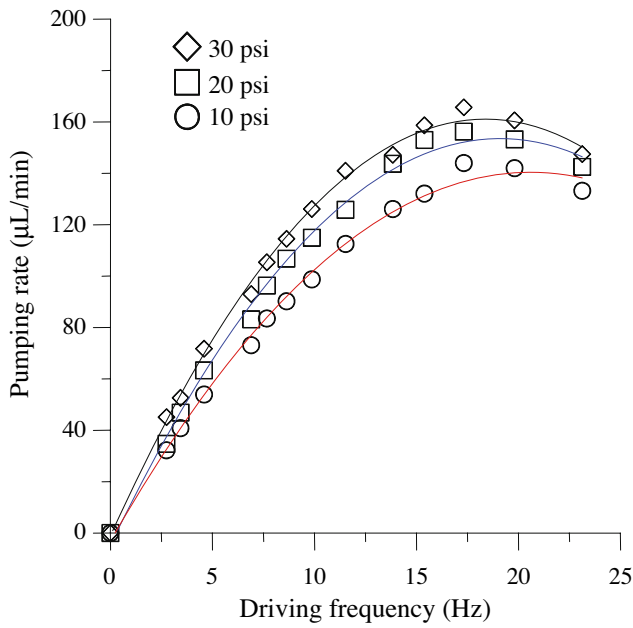


Fig. 6 Relationship between the pumping rate and the driving frequency

The pumping rate can be as high as 165.7 μL/min at a driving frequency of 17 Hz and an air pressure of 30 psi. Furthermore, the venting time increases along with a larger deformation of membrane if the membrane could be de-activated completely during two cycles of deformations. Therefore, the optimum frequency for

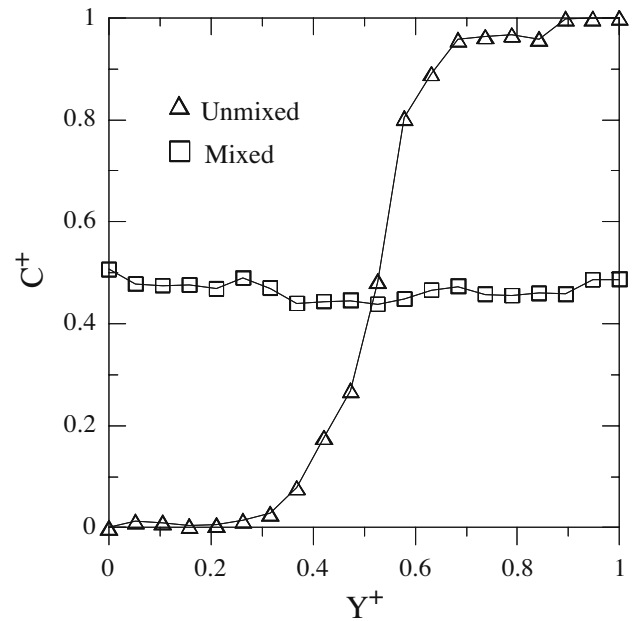
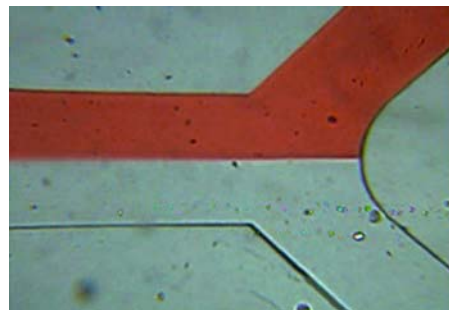


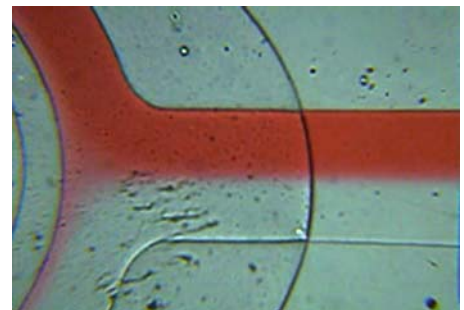
Fig. 8 A comparison of the mixing index with and without using the rotary pump to mix injected samples

maximum pumping rate decreases while the applied pressure increases (as shown in Fig. 6). There will be more fluids driven to increase the pumping rate due to the larger deformation of membrane if the venting time is enough. However, the pumping starts to fall if the driving frequency is too high such that the membrane cannot restore to its

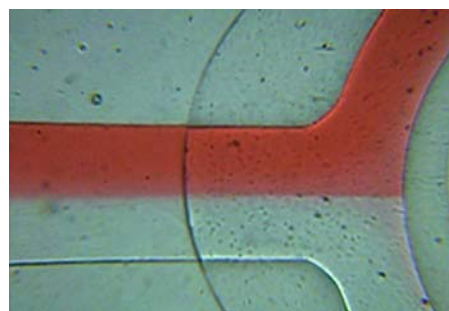
Fig. 7 (a) Image of the confluent flows taken at the X_1 location. Clear separation of two different samples is shown upstream. (b) Downstream image of two different samples showing that the structure of the rotary pump has negligible effect on mixing. (c, d) show a comparison of the unmixed and mixed samples at downstream location (X_3)



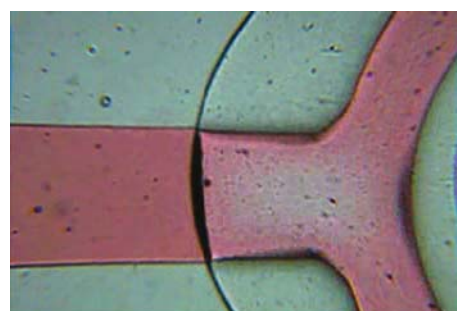
(a) $X=X_1$



(b) $X=X_2$

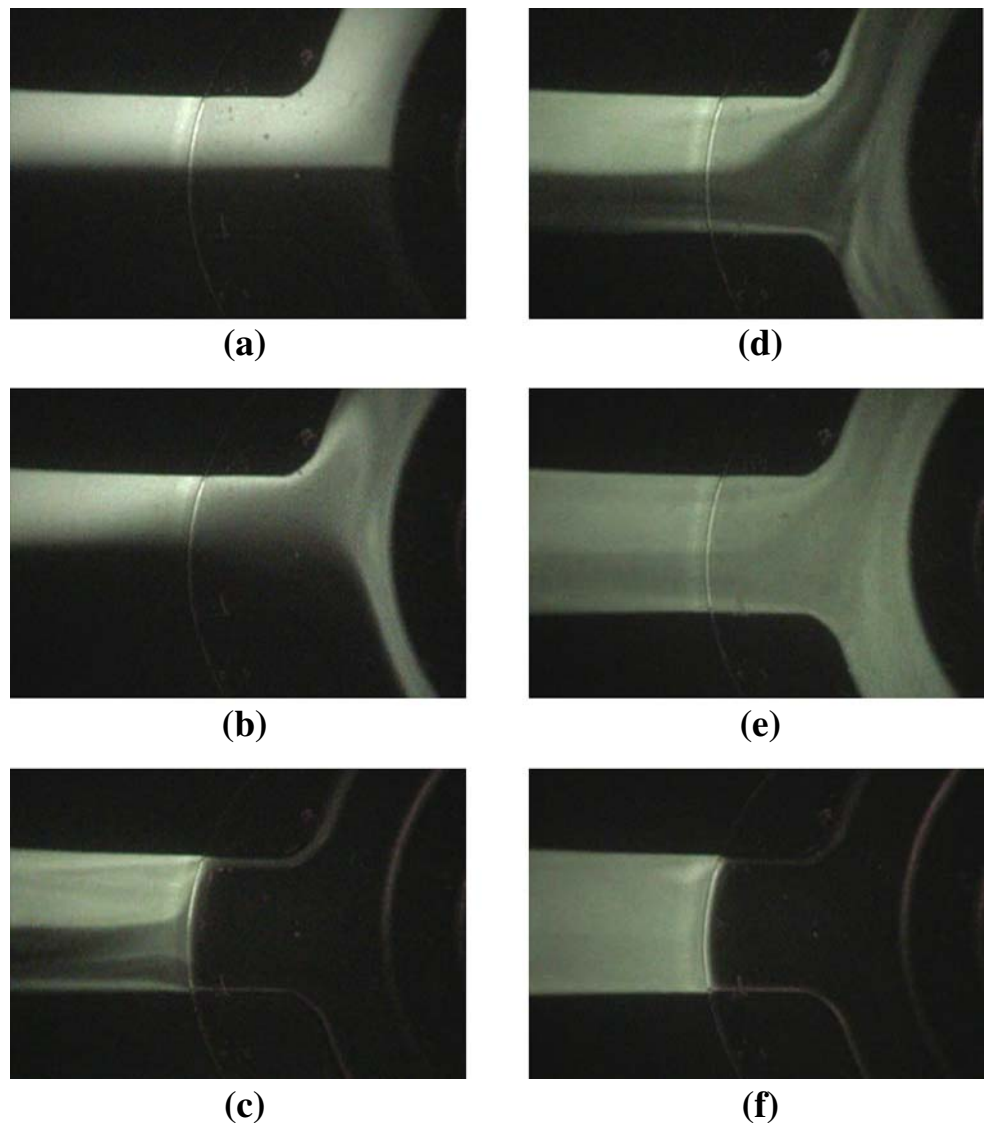


(c) $X=X_3$



(d) $X=X_3$

Fig. 9 A series of images showing the mixing process at (a) $t=0$ s, (b) 0.43 s, (c) $t=0.69$ s, (d) $t=1.42$ s, (e) $t=1.60$ s, and (f) $t=2.07$ s. Note that a cycle in this figure includes a pumping sequence and a mixing sequence



original position. The detail discussion of the optimum driving frequency can be found in our previous work (Huang et al. 2006).

3.2 Characterization of micromixers

Figure 3 schematically illustrates the operation process of the rotary micromixer. The confluent flows can be mixed using an operation sequence (0011, 1001, 1100 and 0110) as described in Section 2.1. As the two different samples, red ink and DI (deionized) water, were injected to the annular fluidic channel, the mixing can be achieved by appropriate sequential activation of the membranes. Figure 7(a), (b) and (c) show the images taken at three different locations (as indicated in Fig. 5). Note that X_1 , X_2 and X_3 are 0.8, 1.7, and 2.3 cm, respectively. Figure 7(a) shows the injection of DI water and ink at the upstream location, indicating that no mixing occurs

while the mixer is not turned on. Figure 7(b) shows that the rotary pump has only a negligible effect on mixing of water and ink. After the two samples merge at the downstream location of the annular channel (X_3), mixing caused by diffusion is still negligible (Fig. 7(c)). After activating the mixer (Fig. 7(d)), samples are mixed significantly.

In order to quantify the performance of the rotary mixer, a mixing index was used and defined as follows (Chang and Yang 2004).

$$\sigma(x) = \left(1 - \frac{\int_0^h |C - C_\infty| dy}{\int_0^h |C_0 - C_\infty| dy} \right) \times 100\% \quad (1)$$

where $\sigma(x)$ is the mixing index regarding a specific concentration across the width of the microchannel. C (subscript 0 or 1) is the initial condition of the unmixed

state, and C_∞ is the completely mixed state (0.5). σ is 100% while the samples are totally mixed and σ is 0%, if the samples are completely unmixed. Experimental data of mixed and unmixed results are shown in Fig. 8. Note that the dye concentration at a location of X_3 was used. The cycle number, applied pressure and driving frequency are 3, 25 psi and 3.46 Hz, respectively. It indicates that while the rotary mixer is turned on, the samples can be well mixed. There is slight mixing across the width of the microchannel due to diffusion before the rotary mixer is turned on. The mixing index of the unmixed condition is calculated to be only 20.4%, and it is enhanced to 93.2% for the mixed condition.

Furthermore, FITC and a buffer solution were used for testing of the micromixer. Figure 9 shows a series of photographs during the mixing process. The frequency of each EMV is 13 Hz and the air pressure is 25 psi. Note that the driving frequency of the rotary mixer (f_{mixing}) was defined as the operation frequency which was calculated from the cycle time of the four membranes. It was calculated from the sequence time of activating the membranes in the annular channel to perform the mixing. Alternatively, the driving frequency of the EMV (f_{EMV}) was the operation frequency applied on the EMV to control the on or off state of the EMV so that the compressed air was supplied to deflect the membrane. Two samples can be completely mixed after three cycles. Images in Fig. 9(a), (b), and (c) correspond to the time at 0, 0.43, and 0.69 s, respectively, at a location of 2.3 cm (X_3). Figure 9(d), (e),

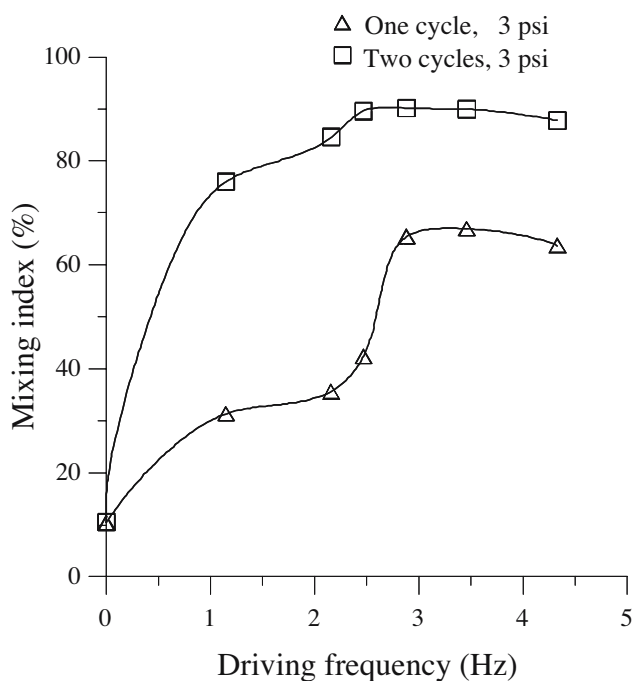


Fig. 10 The relationship between the mixing index and the driving frequency for one-cycle and two-cycle mixing. The optimal frequency is 3.46 Hz

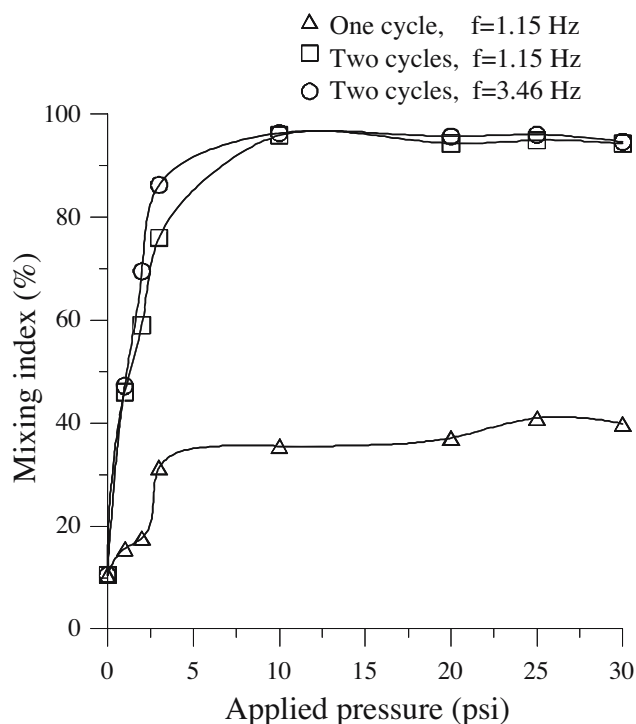


Fig. 11 The relationship between the mixing index and the applied pressure

and (f) are images at 1.42, 1.60, and 2.07 s, respectively. The concentration of the FITC and the CE buffer in the annular channel was shown gradually in Fig. 9(b) (0.43 s), (d) (1.42 s) and (e) (1.60 s) since the images showed significant changes at these moments. Note that the samples cannot be completely mixed at the end of the first cycle as shown in Fig. 9(c). The 10^{-5} M FITC and 10^{-3} M CE buffer were mixed completely after three cycles (2.07 s) as shown in Fig. 9(f). Note that a cycle in Fig. 9 includes a pumping sequence and a mixing sequence. However, a cycle in Figs. 10 and 11 only includes a mixing sequence. The initial mixing index of FITC in Fig. 9(a) is only 10.5%. The mixing performance can be enhanced by increasing the operating time. Experimental data show that the mixing index can be increased from 10.5 to 96.3% after three cycles.

Figure 10 shows the relationship between the mixing index and the driving frequency at a small applied pressure of 3 psi. Experimental data show that the mixing index increases with the driving frequency until it reaches a critical frequency of 3.0 Hz. The mixing index also increases with the cycle number. Notably, rotating confluent fluids along the annular channel for two cycles can generate a maximum mixing index of 90.2%, while one cycle can only generate a value of 67.0%. The mixing index starts to drop at about 4.3 Hz. The optimal driving frequency of the rotary mixer is then determined to range from 3.0 to 4.3 Hz. If the driving frequency is higher than 4.3 Hz, the time that the samples stay in the annular channel is not enough for

better mixing. In other words, samples could not be mixed well in such a short time.

Furthermore, the relationship between the mixing index and the applied pressure is explored and shown in Fig. 11. Since the applied pressure determines the amount of the deformation of the membranes, the mixing index then increases with the applied pressure until the membranes have been completely deformed. For a driving frequency of 1.15 Hz, which is lower than the optimal frequency, the maximum mixing index is 41.0%. This value can be drastically increased to 95.1% by increasing the applied pressure from 3 to 10 psi. Again, the numbers of cycles play an important role on the performance of the micro-mixer. If the mixer is driven at a frequency of 3.46 Hz, the effect of the applied pressure on the mixing index is more prominent. As shown in Fig. 11, if the applied pressure is increased to 3 psi, the mixing index can increase to 86.3% after two cycles. The maximum mixing index can reach a value of 96.3% after 10 psi. Similarly, one cycle is not enough to achieve the complete mixing of samples.

4 Conclusions

This study has demonstrated a new microfluidic rotary device capable of transporting and mixing samples in an annular microchannel. The microfluidic rotary device fabricated by MEMS technology have been successfully used to transport and mix samples. The movement of the fluid in the microchannel is dependent on the actuation of four membranes. The microfluidic rotary device is equipped with two functions. The first function is pumping by using an appropriate operation sequence of the membranes. The second function is the mixing of the pumped fluid in another special sequence. Therefore, samples can be transported and mixed automatically. The pumping rate of this rotary pump increases as air pressure or driving frequency is increased. The performance of the rotary mixer is also investigated in this study. Experimental data show that the mixing index can be increased from 10.5 to 96.3%. Applied air pressure, driving frequency and cycle number affect the mixing index. The developed microfluidic rotary device can perform two functions within a small area. The integration of micropumps and mixers may be useful for the development of miniaturized biomedical and chemical analysis system.

Acknowledgements The authors gratefully acknowledge the financial support provided to this study by the National Science Council, Taiwan (NSC 93-2323-B-006-010), the MOE Program for Promoting Academic Excellence of Universities (EX-91-E-FA09-5-4). Also, the access provided to major fabrication equipment at the Center for Micro/Nano Technology Research, National Cheng Kung University is greatly appreciated.

References

- C.C. Chang, R.J. Yang, *J. Micromechanics Microengineering* **14**, 550 (2004)
- H.P. Chou, M.A. Unger, A. Scherer, S.R. Quake, in *Proceedings of the Solid State Actuator and Sensor Workshop*, 2000
- H.P. Chou, M.A. Unger, S.R. Quake, *Biomed. Microdevices* **3**, 323 (2001)
- D.C. Duffy, H.L. Gillis, J. Lin, N.F. Sheppard, G.J. Kellogg, *Anal. Chem.* **15**, 4669 (1999)
- A.Y. Fu, H.P. Chou, C. Spence, F.H. Arnold, S.R. Quake, *Anal. Chem.* **74**, 2451 (2002)
- I. Glasgow, N. Aubry, *Lab Chip* **3**, 114 (2003)
- P. Gravesen, Y. Branebjerg, O.S. Jensen, *J. Micromechanics Microengineering* **3**, 168 (1993)
- B.L. Gray, D. Jaeggi, N.J. Mourlas, B.P. Van Driehuisen, K.R. Williams, N. Maluf, G.T.A. Kovacs, *Sens. Actuators, A* **77**, 57 (1998)
- S. Hardt, F. Schonfeld, *AIChE J.* **49**, 578 (2003)
- V. Hessel, S. Hardt, H. Lowe, F. Schonfeld, *AIChE J.* **49**, 566 (2003)
- P. Hinsmann, J. Frank, P. Svasek, M. Harasek, B. Lendl, *Lab Chip* **1**, 16 (2001)
- C.C. Huang, S.B. Huang, G.B. Lee, *J. Micromechanics Microengineering* **16**, 2265 (2006)
- B. Husband, M. Bu, A.G.R. Evans, T. Melvin, *J. Micromechanics Microengineering* **14**, 64 (2004)
- H. Katoua, R. Miyakea, K. Kamarab, K. Kawaseb, H. Uchidab, *Chem. Eng. Sci.* **60**, 5519 (2005)
- M. Kochy, D. Chatelainz, A.G.R. Evan, A. Brunnschweiler, *J. Micromechanics Microengineering* **8**, 123 (1998)
- C.Y. Lee, G.B. Lee, L.M. Fu, H.K. Lee, R.J. Yang, *J. Micromechanics Microengineering* **14**, 1390 (2004)
- C.A. Li, T.N. Chen, *Sens. Actuators, B* **106**, 871 (2005)
- Y. Lin, G.J. Gerfen, D.L. Rousseau, S.R. Yeh, *Am. Chem. Soc.* **75**, 5381 (2003)
- J. Liu, M. Enzelberger, S.R. Quake, *Electrophoresis* **23**, 1531 (2002)
- R. Miyake, K. Tsuzuki, T. Takagi, K. Imai, in *The 10th IEEE Workshop on MEMS*, 1997, p. 102
- M.S. Munson, P. Yager, *Anal. Chim. Acta* **507**, 63 (2004)
- N.T. Nguyen, Z. Wu, *J. Micromechanics Microengineering* **15**, 1 (2005)
- S.J. Park, J.K. Kim, J. Park, S. Chung, C. Chung, J.K. Chang, *J. Micromechanics Microengineering* **14**, 6 (2004)
- S.K. Sia, G.M. Whitesides, *Electrophoresis* **24**, 3563 (2003)
- H. Song, M.R. Bringer, J.D. Tice, C.J. Gerdtz, R.F. Ismagilov, *Appl. Phys. Lett.* **83**, 4664 (2003)
- A.D. Stroock, S.K.W. Dertinger, A. Ajdari, I. Mezic, H.A. Stone, G.M. Whitesides, *Science* **295**, 647 (2002)
- H. Suzuki, C.M. Ho, *Microelectromechanical Syst.* **13**, 779 (2004)
- H. Tsai, L. Lin, *Sens. Actuators, A* **97**, 665 (2002)
- M.A. Unger, H.P. Chou, T. Thorsen, A. Scherer, S.R. Quake, *Science* **288**, 113 (2000)
- H.Z. Wang, P. Iovenitti, E. Harvey, S. Masood, *Smart Mater. Struct.* **11**, 662 (2002)
- C.H. Wang, G.B. Lee, *Biosens. Bioelectron.* **21**, 419 (2005)
- A. Yamazaki, M. Sendoh, K. Ishiyama, K.I. Arai, T. Hayase, *IEEE Trans. Magn.* **39**, 3289 (2003a)
- A. Yamazaki, M. Sendoh, K. Ishiyama, T. Hayase, K.I. Arai, *Sens. Actuators, A* **105**, 103 (2003b)
- Z. Yang, H. Goto, M. Matsumoto, R. Maeda, *Electrophoresis* **21**, 116 (2000)
- S. Zeng, C.H. Chen, J.C. Mikkelsen Jr., J.G. Santiago, *Sens. Actuators, B* **79**, 107 (2001)
- B. Ziaie, A. Baldi, M. Lei, Y. Gu, R.A. Siegel, *Adv. Drug Deliv. Rev.* **56**, 145 (2004)